Supplementary Materials

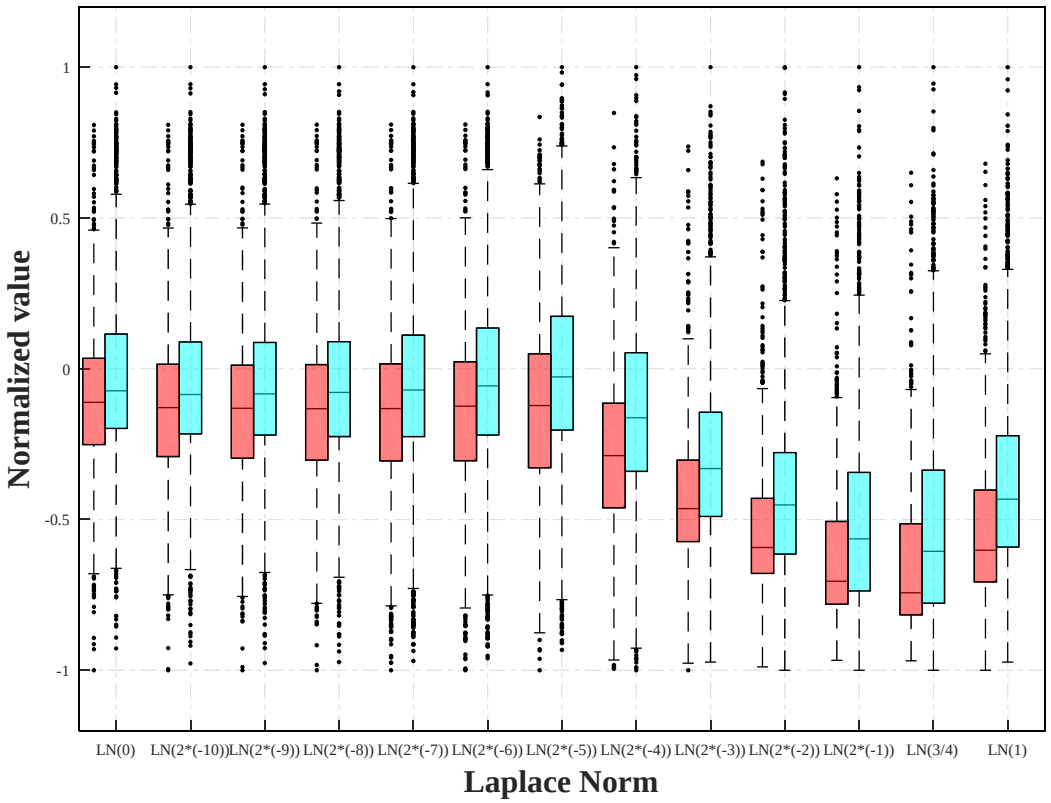

Fig. S1. Comparison of the distribution of Laplacian norms for ligand-binding (red) and non-ligand-binding (cyan) sites by systematical sampling of different scale factors based on the dataset RNA78.

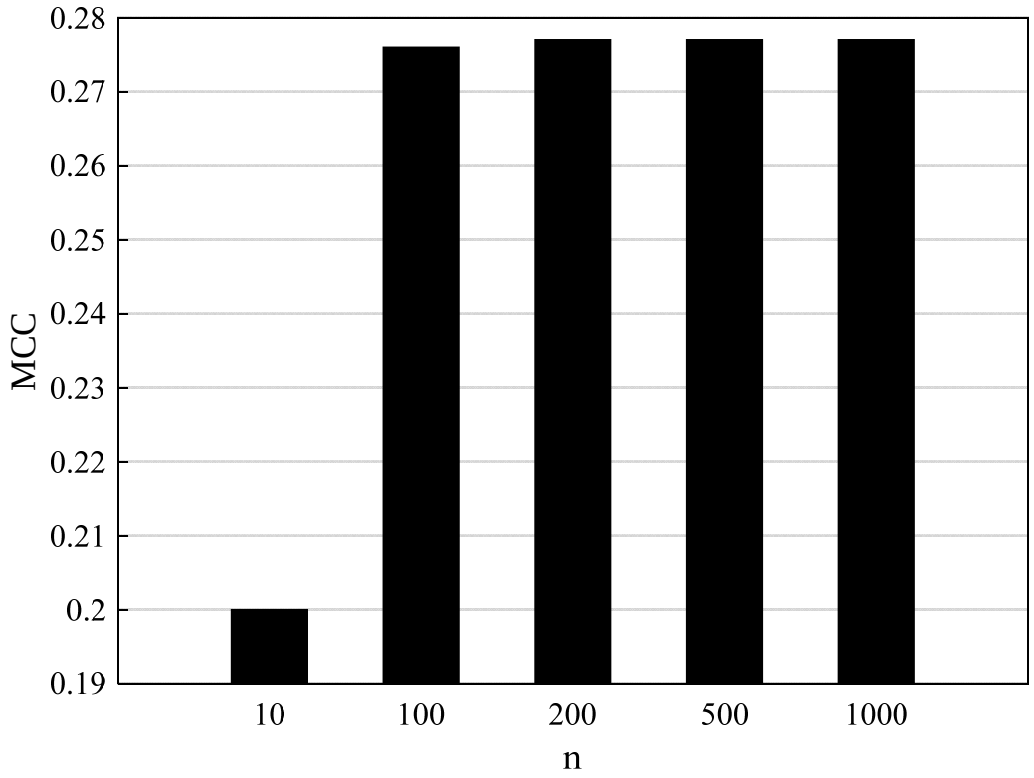

Fig. S2. Optimization of the value of trees *n* in RF based on the 5-fold-CV on the training set TR60.

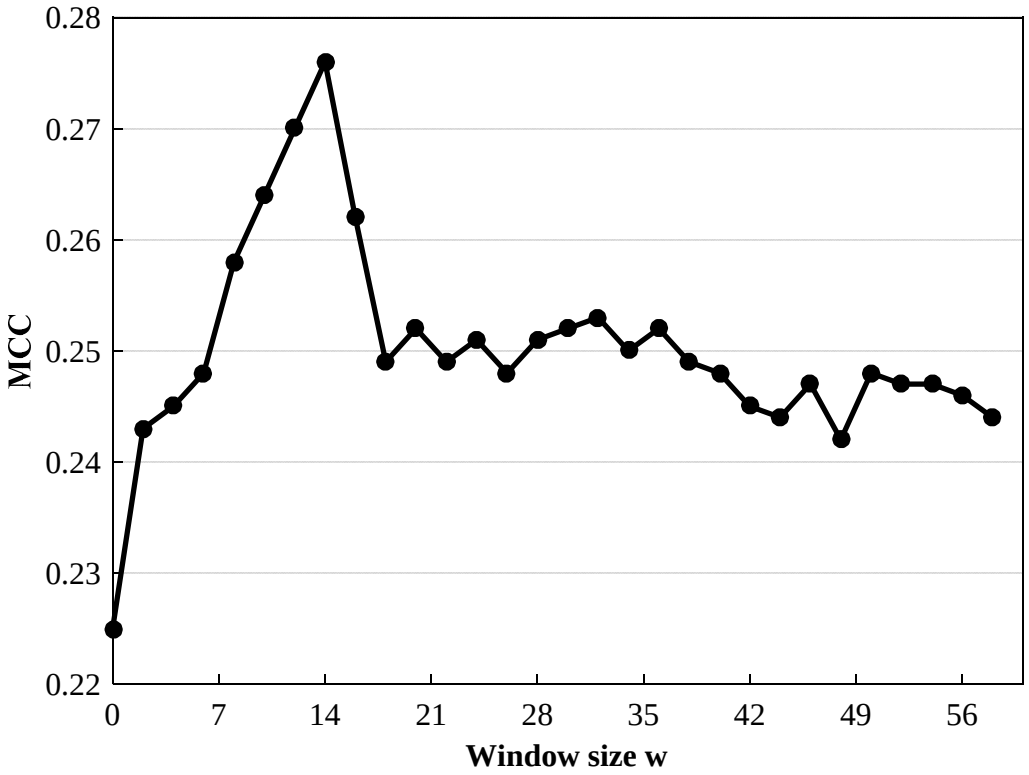

Fig. S3. Optimization of RNAsite_str's window size based on 5-fold-CV on the training set TR60.

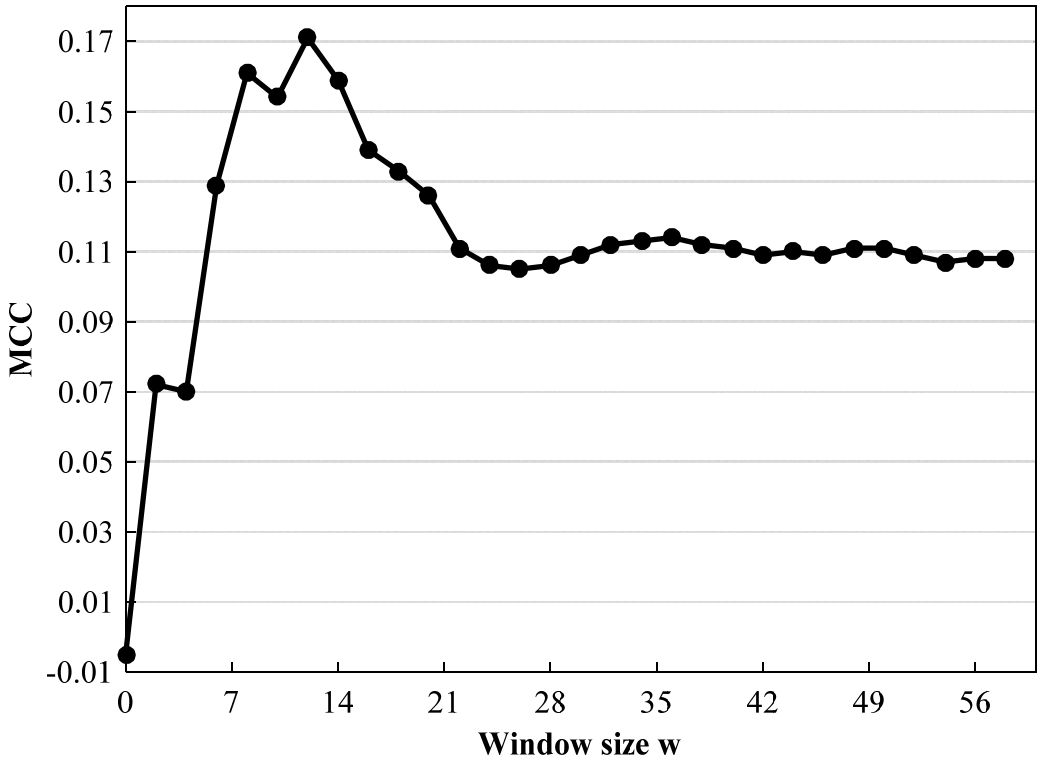

Fig. S4. Optimization of RNAsite_seq's window size based on 5-fold-CV on the training set TR60.

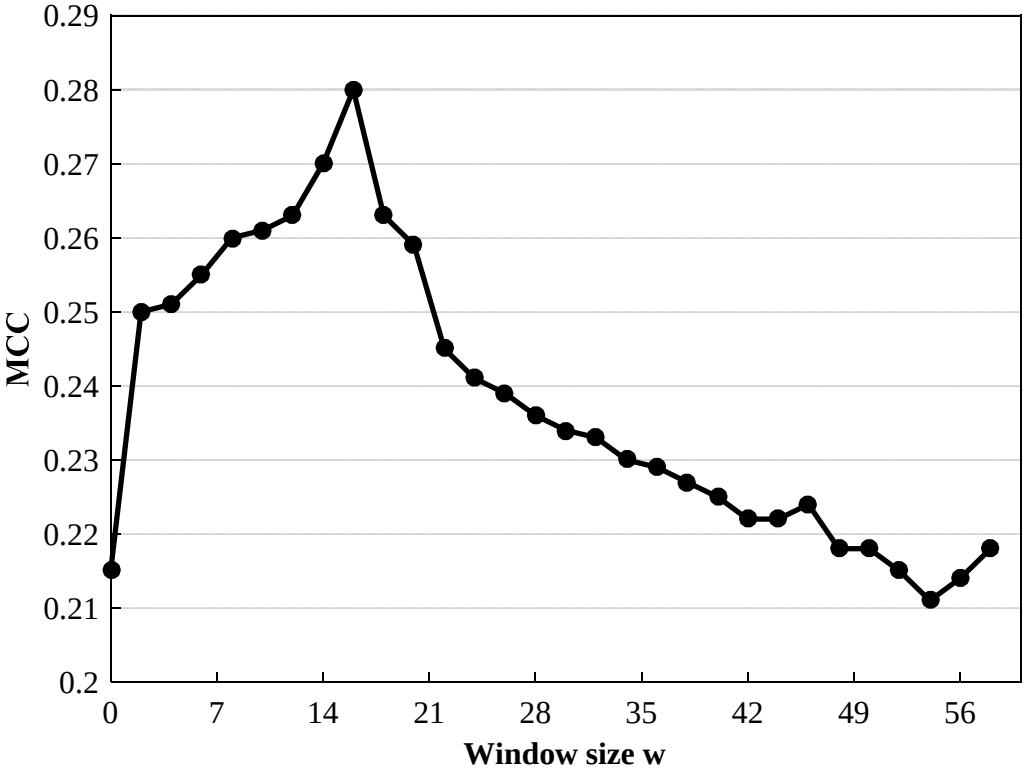

Fig. S5. Optimization of RNAsite's window size based on 5-fold-CV on the training set TR60.

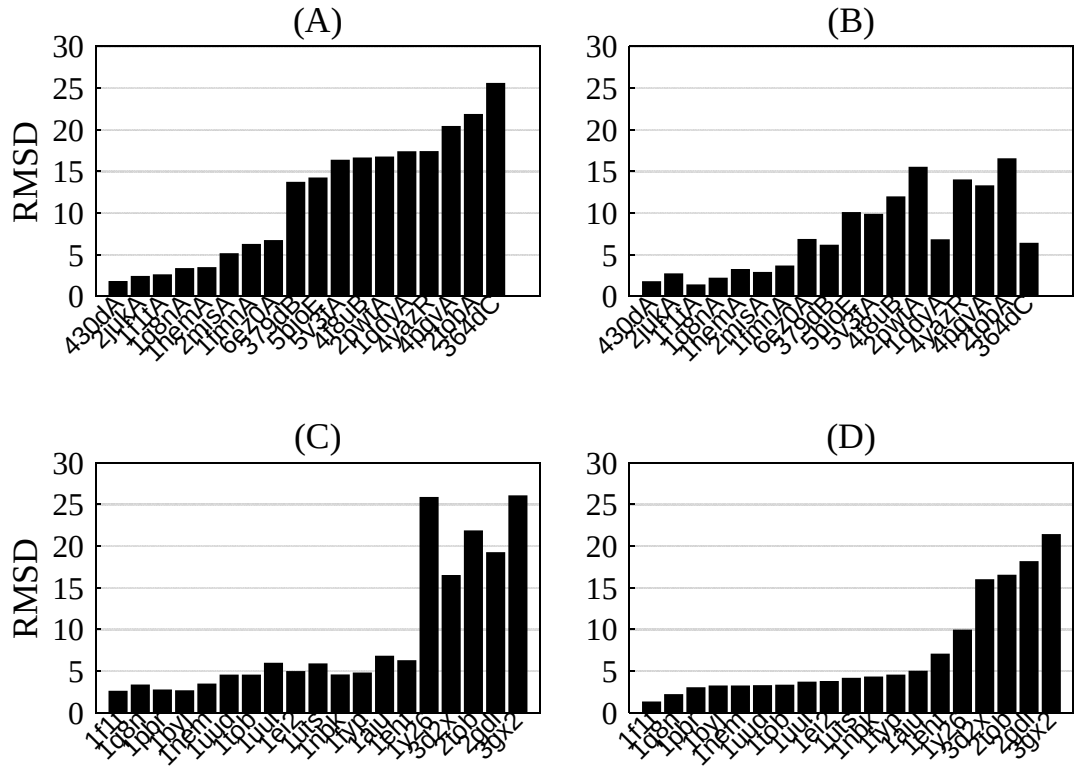

Fig. S6. Accuracy (RMSD) of the modeled structures compared to their native structures. (A) and (B) are respective global and local RMSD of TE18, while (C) and (D) are for RB19.

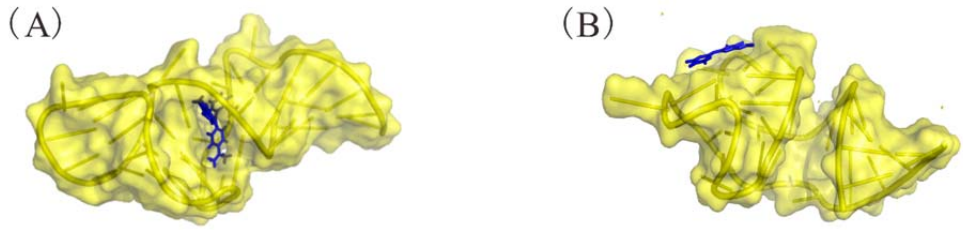

Fig. S7. Two examples to show the location of small molecule in RNA structure. The small molecule and RNA structure are shown in blue sticks and golden surface, respectively. (A) The small molecule is embedded in the concave region of the RNA structure (PDB ID: 1Q8N). (B) The small molecule is attached on the surface of the RNA structure (PDB ID: 5BJO).

Table S1. The details of each structure in TR60. The 'Ligand' column lists the ligand ID and the count of the corresponding ligand in the structure.

Targets	Ligands	RNA structure title
3sktA	MG:2; GNG:1; MN:6;	CRYSTAL STRUCTURE OF THE 2'- DEOXYGUANOSINE RIBOSWITCH
5u3gB	MG:21;	STRUCTURE OF THE DICKEYA DADANTII YKKC RIBOSWITCH BOUND TO GUANIDINIUM
5j02A	MG:49; 6F7:1;	STRUCTURE OF THE LARIAT FORM OF A CHIMERIC DERIVATIVE
2yieZ	FMN:1; MG:6;	CRYSTAL STRUCTURE OF A F. NUCLEATUM FMN RIBOSWITCH BOUND TO FMN
2fcyA	NMY:2;	HIV-1 DIS KISSING-LOOP IN COMPLEX WITH NEOMYCIN
3gx3A	SAH:1; MG:8;	CRYSTAL STRUCTURE OF THE T. TENGCONGENSIS SAM-I RIBOSWITCH
4nybA	MN:4; 2QC:1; MG:9;	CRYSTAL STRUCTURE OF THE E. COLI THIM PYROPHOSPHAE-SPECIFIC (TPP) RIBOSWITCH
1hr2A	MG:17;	CRYSTAL STRUCTURE ANALYSIS OF A MUTANT P4-P6 DOMAIN
4mgmB	MG:9;	CRYSTAL STRUCTURE OF THE IN VITRO TRANSCRIBED G. KAUSTOPHILUS TRNA-GLY
3oxeB	MN:13; GLY:1; MG:5;	CRYSTAL STRUCTURE OF GLYCINE RIBOSWITCH
1y90B	MN:7;	HIV-1 DIS(MAL) DUPLEX MN-SOAKED
2quwB	MG:10;	HAMMERHEAD RIBOZYME G12A MUTANT AFTER CLEAVAGE
4megB	MG:15;	IN VITRO EVOLVED GLMS RIBOZYME TRIPLE MUTANT
4lvxA	H4B:2;	STRUCTURE OF THE THF RIBOSWITCH BOUND TO TETRAHYDROBIOPTERIN
4rgeB	MG:8;	CRYSTAL STRUCTURE OF THE IN-LINE ALIGNED ENV22 TWISTER RIBOZYME
4pcjA	MG:3;	MODIFICATIONS TO TOXIC CUG RNAS INDUCE STRUCTURAL STABILITY AND RESCUE
3c44A	PAR:2;	CRYSTAL STRUCTURE OF HIV-1 SUBTYPE F DIS EXTENDED DUPLEX
5o69A	AG2:1; MG:1;	THE STRUCTURE OF THE THERMOBIFIDA FUSCA GUANIDINE III RIBOSWITCH
2lwkA	0EC:1;	SOLUTION STRUCTURE OF SMALL MOLECULE-INFLUENZA RNA COMPLEX
3vrsA	MN:9;	CRYSTAL STRUCTURE OF FLUORIDE RIBOSWITCH
2g5kA	AM2:2;	CRYSTAL STRUCTURE OF THE HOMO SAPIENS CYTOPLASMIC RIBOSOMAL
5fj1C	MG:3;	THE STANDARD KINK TURN HMKT-7 AS STEM LOOP IN 2 P212121 SPACE GROUP
5d5lD	PRF:1; MG:3;	PREQ1-II RIBOSWITCH WITH AN ENGINEERED G-U WOBBLE PAIR BOUND TO CS+
4frgX	MG:8; I2A:1;	CRYSTAL STRUCTURE OF THE COBALAMIN RIBOSWITCH APTAMER DOMAIN

1ylsB	MG:6; DAI:2;	CRYSTAL STRUCTURE OF SELENIUM-MODIFIED DIELS-ALDER RIBOZYME COMPLEXED
3q50A	PRF:1;	STRUCTURAL ANALYSIS OF A CLASS I PREQ1 RIBOSWITCH APTAMER
4xw7A	AMZ:1; MG:10;	CRYSTAL STRUCTURE OF THE ZMP RIBOSWITCH AT 2.50 ANGSTROM
2ktzA	ISH:1;	INHIBITOR INDUCED STRUCTURAL CHANGE IN THE HCV IRES DOMAIN IIA RNA
4qlmA	MG:2; 2BA:2;	YDAO RIBOSWITCH BINDING TO C-DI-AMP
3fu2A	PRF:1; CA:4;	COCRYSTAL STRUCTURE OF A CLASS-I PREQ1 RIBOSWITCH
5dh8B	ZN:4;	TWO DIVALENT METAL IONS AND CONFORMATIONAL CHANGES PLAY ROLES
3meiB	MG:3;	REGULATORY MOTIF FROM THE THYMIDYLATE SYNTHASE MRNA
6fz0A	SAM:1; MG:1;	CRYSTAL STRUCTURE OF THE METY SAM V RIBOSWITCH
2mxsA	PAR:1;	SOLUTION NMR-STRUCTURE OF THE NEOMYCIN SENSING RIBOSWITCH RNA
2nokC	MN:3; MG:2;	CRYSTAL STRUCTURE OF AN RNA DOMAIN FROM HEPATITIS C VIRUS.
1ajuA	ARG:1;	HIV-2 TAR-ARGININAMIDE COMPLEX
1fypA	PAR:1;	EUKARYOTIC DECODING REGION A-SITE RNA-PAROMOMYCIN COMPLEX
4k31C	AM2:4;	CRYSTAL STRUCTURE OF APRAMYCIN BOUND TO THE LEISHMANIAL RRNA A-SITE
2nokB	MG:4;	CRYSTAL STRUCTURE OF AN RNA DOMAIN FROM HEPATITIS C VIRUS.
1ntbA	MG:1; SRY:1;	2.9 A CRYSTAL STRUCTURE OF STREPTOMYCIN RNA-APTAMER COMPLEX
3bnqC	PAR:1;	CRYSTAL STRUCTURE OF THE HOMO SAPIENS MITOCHONDRIAL
5vciA	8OS:1;	RNA HAIRPIN STRUCTURE CONTAINING TETRALOOP/RECEPTOR MOTIF
3q3zV	C2E:2; MG:6;	STRUCTURE OF A C-DI-GMP-II RIBOSWITCH FROM C. ACETOBUTYLICUM
1uudB	P14:1;	NMR STRUCTURE OF A SYNTHETIC SMALL MOLECULE
1byjA	GE1:1; GE3:1; GE2:1;	GENTAMICIN C1A A-SITE COMPLEX
1lvjA	PMZ:1;	STRUCTURE OF TAR RNA COMPLEXED WITH A TAT-TAR INTERACTION
1utsB	P13:1;	DESIGNED HIV-1 TAR BINDING LIGAND
1qd3A	BDG:1; RIB:1; CYY:1; IDG:1;	HIV-1 TAR RNA/NEOMYCIN B COMPLEX
1arjN	ARG:1;	ARG-BOUND TAR RNA
2l8hA	ARG:1; L8H:1;	CHEMICAL PROBE BOUND TO HIV TAR RNA
6hagA	SAH:1;	THE STRUCTURE OF THE SAM/SAH-BINDING RIBOSWITCH.

1yrjA	AM2:2; MG:1;	CRYSTAL STRUCTURE OF APRAMYCIN BOUND TO A RIBOSOMAL RNA A SITE
1tobA	TOC:1; TOA:1; TOB:1;	SACCHARIDE-RNA RECOGNITION IN AN AMINOGLYCOSIDE ANTIBIOTIC-
1f1tA	ROS:1;	CRYSTAL STRUCTURE OF THE MALACHITE GREEN APTAMER COMPLEXED
3tzrA	SS0:1; MG:5;	STRUCTURE OF A RIBOSWITCH-LIKE RNA-LIGAND COMPLEX FROM THE HEPATITIS C
4qjhC	MG:3;	CRYSTAL STRUCTURE OF THE TWISTER RIBOZYME
2kgpA	MIX:1;	STRUCTURAL BASIS FOR STABILIZATION OF THE TAU PRE-MRNA SPLICING
1rawA	AMP:1;	ATP BINDING RNA APTAMER IN COMPLEX WITH AMP
1ehtA	TEP:1;	THEOPHYLLINE-BINDING RNA IN COMPLEX WITH THEOPHYLLINE
1nbkA	GND:2;	THE STRUCTURE OF RNA APTAMER FOR HIV TAT COMPLEXED WITH TWO
1ei2A	NMY:1;	STRUCTURAL BASIS FOR RECOGNITION OF THE RNA MAJOR GROOVE IN THE TAU

Table S2. The details of each structure in TE18. The ‘Ligand’ column lists the ligand ID and the count of the corresponding ligand in the structure.

Targets	Ligands	RNA structure title
2pwtA	LHA:3;	CRYSTAL STRUCTURE OF THE BACTERIAL RIBOSOMAL DECODING SITE
5v3fA	74G:1;	CO-CRYSTAL STRUCTURE OF THE FLUOROGENIC RNA MANGO
379dB	CO:4;	THE STRUCTURAL BASIS OF HAMMERHEAD RIBOZYME SELF-CLEAVAGE
5bjoE	MG:2; 747:1;	CRYSTAL STRUCTURE OF THE CORN RNA APTAMER IN COMPLEX WITH DFHO
4pqvA	MG:7;	CRYSTAL STRUCTURE OF AN XRN1-RESISTANT RNA FROM THE 3' UNTRANSLATED
430dA	MG:9;	STRUCTURE OF SARCIN/RICIN LOOP FROM RAT 28S RRNA
1nemA	BDR:1; BDG:1; NEB:1; IDG:1;	SACCHARIDE-RNA RECOGNITION IN THE NEOMYCIN B / RNA APTAMER
1q8nA	MGR:1;	SOLUTION STRUCTURE OF THE MALACHITE GREEN RNA BINDING
1f1tA	ROS:1;	CRYSTAL STRUCTURE OF THE MALACHITE GREEN APTAMER COMPLEXED
2jukA	G0B:1;	GUANIDINO NEOMYCIN B RECOGNITION OF AN HIV-1 RNA HELIX
4yazR	4BW:1; MG:4;	3'-CGAMP RIBOSWITCH BOUND WITH 3'
364dC	MG:8;	3.0 A STRUCTURE OF FRAGMENT I FROM E. COLI 5S RRNA
6ez0A	U37:5;	SPECIFIC PHOSPHOROTHIOATE SUBSTITUTION WITHIN DOMAIN 6 OF A GROUP II
2tobA	TOA:1; 2TB:1; TOC:1;	SOLUTION STRUCTURE OF THE TOBRAMYCIN-RNA APTAMER COMPLEX
1ddyA	B12:1; NME:1;	MOLECULAR RECOGNITION BY THE VITAMIN B12 RNA APTAMER
1fmnA	FMN:1;	SOLUTION STRUCTURE OF FMN-RNA APTAMER COMPLEX
2misA	MG:4;	NMR LOCALIZATION OF DIVALENT CATIONS AT THE ACTIVE SITE
4f8uB	SIS:2;	CRYSTAL STRUCTURE OF THE BACTERIAL RIBOSOMAL DECODING SITE IN COMPLEX

Table S3. The details of each structure in RB19. The 'Ligand' column lists the ligand ID and the count of the corresponding ligand in the structure.

Target	Ligand	RNA structure title
1aju	ARG:1	HIV-2 TAR-ARGININAMIDE COMPLEX
1byj	GE1:1; GE3:1; GE2:1	GENTAMICIN C1A A-SITE COMPLEX
1eht	TEP:1	THEOPHYLLINE-BINDING RNA IN COMPLEX WITH THEOPHYLLINE
1ei2	NMY:1	STRUCTURAL BASIS FOR RECOGNITION OF THE RNA MAJOR GROOVE IN THE TAU
1f1t	ROS:1; SR(artifact):3	CRYSTAL STRUCTURE OF THE MALACHITE GREEN APTAMER COMPLEXED
1fyp	PAR:1	EUKARYOTIC DECODING REGION A-SITE RNA-PAROMOMYCIN COMPLEX
1nbk	GND:2	THE STRUCTURE OF RNA APTAMER FOR HIV TAT COMPLEXED
1nem	NEB:1; IDG:1; BDG:1; BDR:1	SACCHARIDE-RNA RECOGNITION IN THE NEOMYCIN B / RNA APTAMER
1pbr	IDG:1; PA1:1; BDR:1; CYY:1	STRUCTURE OF 16S RIBOSOMAL RNA
1q8n	MGR:1	SOLUTION STRUCTURE OF THE MALACHITE GREEN RNA BINDING
1tob	TOB:1; TOC:1; TOA:1	SACCHARIDE-RNA RECOGNITION IN AN AMINOGLYCOSIDE ANTIBIOTIC-
1uts	P13:1	DESIGNED HIV-1 TAR BINDING LIGAND
1uud	P14:1	NMR STRUCTURE OF A SYNTHETIC SMALL MOLECULE
1uui	P12:1	NMR STRUCTURE OF A SYNTHETIC SMALL MOLECULE
1y26	MG:2; ADE:1	A-RIBOSWITCH-ADENINE COMPLEX
2gdi	NA(artifact):2; MG:3; TPP:1; K(artifact):3	CRYSTAL STRUCTURE OF THIAMINE PYROPHOSPHATE-SPECIFIC RIBOSWITCH IN COMPLEX
2tob	2TB:1; TOC:1; TOA:1	SOLUTION STRUCTURE OF THE TOBRAMYCIN-RNA APTAMER COMPLEX
3d2x	MG:6; D2X:1	STRUCTURE OF THE THIAMINE PYROPHOSPHATE-SPECIFIC RIBOSWITCH
3gx2	MG:5; SFG:1	TTESAM-I RIBOSWITCH VARIANT A94GU34C BOUND TO SINEFUNGIN

Table S4. Comparison with existing methods on the TE18 dataset.

Methods	MCC	Precision	Recall	AUC
Rsite2	0.01	0.37	0.214	0.474
Rsite^{m}	0.055	0.444	0.293	0.496
Rsite	0.071	0.449	0.288	0.509
RBind^{m}	0.141	0.560	0.139	0.540
RBind	0.187	0.655	0.173	0.559
RNAsite_seq	0.16	0.481	0.294	0.641
RNAsite_str^{m}	0.185	0.513	0.321	0.695
RNAsite_str	0.25	0.67	0.265	0.769
RNAsite^{m}	0.186	0.515	0.317	0.703
RNAsite	0.253	0.675	0.263	0.776

Note: ^{m} denotes that the modeled structures were used.

Table S5. Comparison with existing methods on the RB19 dataset.

Methods	MCC	Precision	Recall	AUC
Rsite2	0.099	0.39	0.279	0.529
Rsite^{m}	0.051	0.356	0.279	0.496
Rsite	0.103	0.394	0.33	0.513
RBind^{m}	0.187	0.554	0.180	0.558
RBind	0.315	0.796	0.239	0.597
RNAsite_seq	0.508	0.684	0.606	0.801
RNAsite_str^{m}	0.445	0.663	0.534	0.806
RNAsite_str	0.557	0.750	0.633	0.874
RNAsite^{m}	0.526	0.677	0.620	0.834
RNAsite	0.567	0.754	0.647	0.877

Note: ^{m}denotes that the modeled structures were used.

Table S6. Comparison of predictive performance of static features and dynamic features of RNA structure on TE18.

Methods	MCC	Pre	Rec	AUC
RNAsite	0.253	0.675	0.263	0.776
D1_RNAsite	0.249	0.653	0.276	0.763
D5_RNAsite	0.246	0.649	0.273	0.76

Note: D1_RNAsite and D5_RNAsite indicate adding two additional features (CL and DG) from one alternative structural configuration, and ten additional features from five alternative structural configurations extracted from the trajectory, respectively.

Table S7. The *p*-values of the statistical tests for the data in Figure 3. The meaning of each feature group: (1) SS, (2) SA, (3) DG, (4) CL, (5) LN, (6) LN+CL, (7) LN+CL+DG, (8) LN+CL+DG+SA, (9) ALL (i.e., LN+CL+DG+SA+SS). The '+'/'-' sign in the lower triangle indicates that the MCC for the feature groups from the row is higher/lower than the one from the corresponding column.

Feature	1	2	3	4	5	6	7	8	9
1		0.0006	7.2*10-7	2.9*10-7	4.8*10-8	1.7*10-9	2.5*10-9	2.4*10-9	2.4*10-9
2	+		1.4*10-6	1.9*10-7	4.6*10-8	2.8*10-10	2.9*10-10	6*10-10	6.6*10-10
3	+	+		0.0315	4.9*10-6	6.7*10-7	6*10-7	1.8*10-7	1.8*10-7
4	+	+	+		2.7*10-5	4*10-5	6.8*10-7	5*10-7	4.6*10-5
5	+	+	+	+		0.03	0.0011	4.8*10-5	5*10-5
6	+	+	+	+	+		0.0033	0.0001	0.0001
7	+	+	+	+	+	+		0.001	0.001
8	+	+	+	+	+	+	+		0.3732
9	+	+	+	+	+	+	+	-	

Table S8. The *p*-values of the statistical tests for the data in Table S3 based on MCC. The '+'/'-' sign in the lower triangle indicates that the MCC for the method from the row is higher/lower than the one from the corresponding column.

Methods	Rsite^{m}	Rsite2	Rsite	RBind^{m}	RNAsite_seq	RNAsite^{m}	RNAsite_str^{m}	RBind	RNAsite_str	RNAsite
Rsite^{m}		0.002	3.6*10-5	0.0098	9.3*10-5	1.4*10-7	1.7*10-7	3.3*10-7	9.1*10-8	2.2*10-10
Rsite2	+		0.3325	0.5819	0.0186	1.9*10-7	1.8*10-6	3.7*10-5	2*10-6	4.2*10-8
Rsite	+	+		0.0516	0.0042	0.0001	3.1*10-6	1.9*10-6	5.6*10-8	7.8*10-11
RBind^{m}	+	+	-		0.0001	4.7*10-5	1.6*10-6	6.2*10-7	1.3*10-8	1.7*10-9
RNAsite_seq	+	+	+	+		0.0333	0.0003	0.0022	6.2*10-7	4.8*10-7
RNAsite^{m}	+	+	+	+	+		0.0087	0.214	0.0002	2.5*10-5
RNAsite_str^{m}	+	+	+	+	+	+		0.2923	0.0013	0.0009
RBind	+	+	+	+	+	+	+		7.9*10-6	1.7*10-6
RNAsite_str	+	+	+	+	+	+	+	+		0.0758
RNAsite	+	+	+	+	+	+	+	+	+	

Table S9. The *p*-values of the statistical tests for the data in Table S4 based on MCC. The '+'/'-' sign in the lower triangle indicates that the MCC for the method from the row is higher/lower than the one from the corresponding column.

Methods	Rsite^{m}	Rsite2	Rsite	RBind^{m}	RNAsite_seq	RNAsite^{m}	RNAsite_str^{m}	RBind	RNAsite_str	RNAsite
Rsite^{m}		0.0001	0.0015	6*10-8	2.9*10-9	1.3*10-10	3.9*10-10	1.3*10-10	7.5*10-12	2.5*10-12
Rsite2	+		0.895	4.3*10-7	1.6*10-10	6.2*10-12	1.1*10-9	3.1*10-8	1*10-10	8.3*10-12
Rsite	+	+		1.2*10-6	4.1*10-11	1.8*10-10	4.9*10-9	1.5*10-11	6.5*10-15	2.3*10-14
RBind^{m}	+	+	+		3.8*10-9	4.9*10-9	2.7*10-7	1.2*10-6	1*10-10	4.7*10-11
RNAsite_seq	+	+	+	+		0.0005	0.0005	2.4*10-6	0.0007	8.8*10-5
RNAsite^{m}	+	+	+	+	+		2.5*10-5	1.9*10-6	0.1032	0.1546
RNAsite_str^{m}	+	+	+	+	-	-		0.0004	1.3*10-5	2.1*10-6
RBind	+	+	+	+	-	-	-		3.7*10-10	8*10-10
RNAsite_str	+	+	+	+	-	+	+	+		0.1231
RNAsite	+	+	+	+	-	+	+	+	+	

Table S10. Comparison between our method and DCA. The comparison is based on 4 RNAs which DCA returned results. RNAsite is based on predicted RNA structure. *L* is the length of a target RNA. The top-ranked nucleotide pairs are regarded as binding small molecules.

Method	**MCC**	**Precision**	**Recall**	**AUC**
DCA (*L*/10)	0.011	0.229	0.132	0.499
DCA (*L*/5)	0.071	0.248	0.299	0.516
DCA (*L*/2)	-0.066	0.198	0.396	0.351
RNAsite_seq	0.086	0.405	0.091	0.6
RNAsite	0.134	0.341	0.197	0.65

Table S11. Comparison between our method and InfoRNA. The comparison is based on 7 RNAs which the InfoRNA server returned results. RNAsite is based on predicted RNA structure.

Method	**MCC**	**Precision**	**Recall**	**AUC**
InfoRNA	-0.169	0.291	0.082	0.412
RNAsite_seq	0.028	0.474	0.183	0.609
RNAsite	0.144	0.555	0.232	0.663

Table S12. Comparison of predictive performance of RNAsite_str based on native structures on three test subsets of TE18. The first (denoted by sub1) contains 4 RNAs with metal ions only. The second (denoted by sub2) contains containing 12 RNAs without any metal ions. The third (denoted by sub3) contains 2 RNAs with both metal ions and non-metal ion small-molecules.

Dataset (type, size of subset)	**MCC**	**Precision**	**Recall**	**AUC**
sub1 (metal ions only, 4)	0.058	0.42	0.213	0.577
sub2 (no metal ions, 12)	0.304	0.625	0.395	0.715
sub3 (mixed, 2)	0.193	0.422	0.296	0.649